An efficient direct arylation polycondensation via C-S bond cleavage

Meng Zhang
University of Chinese Academy of Sciences
Bei-Bei Zhang
University of Chinese Academy of Sciences
Qijie Lin
University of Chinese Academy of Sciences
ziling jiang
Jianqi Zhang
National Center for Nanoscience and Technology https://orcid.org/0000-0002-3549-1482
Yawen Li
Institute of Chemistry, Chinese Academy of Sciences https://orcid.org/0000-0001-5902-6828
Shurui Pei
University of Chinese Academy of Sciences
Xiao Han
University of Chinese Academy of Sciences
Haigen Xiong
University of Chinese Academy of Sciences
Xinyu Liang
University of Chinese Academy of Sciences
Yuze Lin
Institute of Chemistry, Chinese Academy of Sciences https://orcid.org/0000-0002-0325-3842
Zhixiang Wei
National Center for Nanoscience and Technology https://orcid.org/0000-0001-6188-3634
Fengjiao Zhang
University of Chinese Academy of Sciences
Xin Zhang
University of Chinese Academy of Sciences https://orcid.org/0000-0002-4611-0286
Zhixiang Wang
Graduate University of the Chinese Academy of Sciences https://orcid.org/0000-0001-5815-3032
Qinqin Shi
University of Chinese Academy of Sciences
Hui Huang (huihuang@ucas.ac.cn)
University of Chinese Academy of Sciences https://orcid.org/0000-0002-6102-2815

Article

Keywords:

Posted Date: March 14th, 2023

DOI: https://doi.org/10.21203/rs.3.rs-2665169/v1

Abstract

The direct arylation polycondensation (DArP) has become one of the most important methods to construct conjugated polymers (CPs). However, the homocoupling side-reactions of environmentally-harmful aryl halides and the low regioseletive reactivities of unfunctionalized aryls hinder the development of DArP. Here, we report an efficient Pd and Cu co-catalysis DArP was presented via inert C-S bond cleavage of electron rich aryl thioethers, of which robustness was exemplified by over twenty conjugated polymers (CPs), including copolymers, homopolymers, and random polymers.The capture of oxidative addition intermediate together with experimental and theoretic results suggested the important role of palladium (Pd) and copper (Cu) co-catalysis with a bicyclic mechanism. The studies of NMR, molecular weights, trap densities, X-ray diffraction, and the charge transport mobilities revealed this method is an excellent choice for synthesizing CPs.

Introduction

The conjugated polymers (CPs), usually prepared by transition-metal catalyzed cross-coupling polymerization, are indispensable functional materials for organic biomedical and optoelectronic devices, such as biophotonics[1], organic photovoltaics (OPVs)[2–4], organic light-emitting diodes (OLEDs)[5], and organic field-effect transistors (OFETs)[6–8]. Unfortunately, the typical cross-coupling polycondensations, such as Suzuki[9,10], Stille[11], and Negishi[12], generally require the pre-functionalization of monomers, which increased the synthetic complexity and the cost of the CPs. Therefore, the direct arylation polycondensation (DArP) (Fig. 1a) has been developed as an atom-economical method to synthesize CPs[13–15], which usually employed aromatic halides as electrophiles and unfunctionalized aryls as nucleophiles[16–19]. However, the halogenated aryls are environmentally harmful and restrained in substrates scope[20]. More importantly, the homocoupling of halides electrophiles possibly result in inseparable structural defects in the resultant CPs, detrimental to their properties[21,22]. Also, the low regioselective reactivity of the unfunctionalized aryls usually led to branching reactions, affording CPs with low molecular weights and yields[23]. Therefore, it is urgent to explore efficient DArP methods to precisely synthesize CPs with renewable and sustainable electrophiles[24].

Among various C-heteroatom bonds cleavage based catalysis, the transition metal catalysis via C-S bond cleavage is unique and critical[25]. First, the organosulfur compounds can be accessed due to the wide existence in natural products[26], pharmaceuticals[27], and materials[28]. Second, the orthogonal reactivity between the C-S and other C-heteroatom bonds provided opportunities for simplifying the synthetic routes[29,30]. Nevertheless, most transition metals can be strongly bounded with sulfur-containing compounds, causing catalyst poisoning or substrate decomposition[31,32]. Thus, transition-metal catalyzed cross-coupling reactions via direct C-S bond cleavage is still at infancy stage[25]. Recently, the first carbon-sulfur bond activation based polymerization (CASP) of the aryl thioethers and aryl stannanes were reported for precise synthesis of CPs (Fig. 1b)[33]. However, the toxicity of the tin-reagents obviously hindered the large-scale application. Also, the catalytic mechanism is still elusive.

Here, a DArP method via C-S bond cleavage of aryl thioethers (Fig. 1c) was exploited to synthesize CPs with high regioselectivity. The robustness and generality of this methodology were exemplified with over twenty CPs including copolymers, homopolymers, and random polymers, synthesized by a broad array of (hetero)aryls and electron rich aryl thioethers. Furthermore, comprehensively experimental and theoretical studies revealed the important role of palladium (Pd) and copper (Cu) cocatalysis with a bicyclic mechanism, supported by the isolation of oxidative addition intermediate, deuterium experiments, and DFT calculations. Importantly, the direct comparison of NMR, molecular weights, trap densities, and charge transport mobilities of the polymers revealed our method is efficient in synthesizing CPs.

Result And Discussion

Optimization of Small Molecule Reaction Conditions

A model reaction using 4-hexyl-2-(methylthio)thiophene (**1a**) and benzo[*b*]thiophene (**2**) as coupling partners was performed (Table 1 and Supplementary Table 1, 2). The initial test using Herrmann's catalyst (5 mol%) and a bidentate phosphorus ligand (dcype, 10 mol%) under a basic condition in toluene produced 2-(4-hexylthiophen-2-yl)benzo[*b*]thiophene (**3a**) in 45% yield (entry 1, Table 1). To further enhance the efficiency, various copper salts were screened (Supplementary Table 1)[34-38]. Gratifyingly, the yield was improved to 78% in the presence of CuI (entry 2, Table 1), suggesting the important role of copper salts. Next, various Pd catalysts were scrutinized (entries 3-5, Table 1). As a result, $Pd_2(dba)_3$ offered a high yield up to 91% in GC analysis (entry 3, Table 1), and an isolated yield of 85%. Importantly, the low loading of $Pd_2(dba)_3$ (entries 6 and 7, Table 1) afforded **3a** in excellent yields up to 98% and 93%, respectively. The slightly low conversion in entry 3 for this arylation substitution may be due to the homocoupling reaction from **1a** (Supplementary Fig. 1). After replacing **1a** with thioanisole (**1b**), the **1b** is barely homocoupling in comparison with **1a** (Supplementary Fig. 2). Under the similar condition as entry 6, the cross-coupling reaction between **1b** and **2** afforded 2-phenylbenzo[*b*]thiophene (**3b**) in 45% yield (entry 8, Table 1). Thus, Pd catalysts were further screened. Interestingly, the reaction with $Pd(MeCN)_2Cl_2$ or $Pd(P^tBu_3)_2$ (entries 9 and 10, Table 1) as the catalyst produced **3b** in good yields (77% - 88%). However, reducing the loading of $Pd(P^tBu_3)_2$ to 5 mol% dramatically lowered the yield of **3b** to 37% (entry 11, Table 1). Additional screen on metal catalysts, ligands, and solvents was summarized in Supplementary Table 1, which revealed that entry 10 (Table 1) is the optimal reaction condition for **1b**. Furthermore, the screen on the electron deficient aryl thioethers (Supplementary Fig. 3), such as 2-(methylthio)benzo[*d*]oxazole (**1c**), showed no reactivity under this optimal condition, indicating the activation of C-S bond in this reaction may undergo a different mechanism from the previous copper-coordination activation pathway[39]. To understand the selectivity of C-H activation of (hetero)aryls, a detailed gas chromatography-mass spectrometry (GC-MS) analysis on the byproducts between the coupling of **1b** and **2** was conducted. Significantly, no benzyl substitution at C3 position of **2** was observed (Supplementary Fig. 4), suggesting that this methodology possesses little chance to form branching defects in CPs.

Mechanistic Studies

To elucidate the mechanism of this Pd/Cu dual-catalyzed C-H/C-S activation reaction, a series of mechanistic studies were performed. Initially, an oxidative addition product **A** (Supplementary Fig. 5) from the reaction of **1a** with $Pd_2(dba)_3$/dcype was identified by ^{31}P NMR spectroscopy with two new downfield peaks (δ =56.7, 55.4 ppm), suffering from poor isolation. Pleasantly, a product **B** of the oxidative addition of $Pd(P^tBu_3)_2$/dcype to **1b** in toluene at 110 ^oC was successfully isolated in 54% yield (Fig. 2a). The structure of complex **B** was characterized by electrospray ionization-mass spectrometry (ESI-MS) (Supplementary Fig. 6, $[M+Na]^+$ mass-to-charge ratio (*m/z*) = 675.2523), ^1H and ^{31}P NMR spectroscopy with two new downfield peaks (δ = 61.3, 60.3 ppm). More importantly, the single crystal X-ray structure analysis revealed that the Pd atom of **B** is in a square-planar geometry with the dcype ligand coordinating in a *cis*-configuration (Fig. 2a). Note that the oxidative intermediate can be adopted to consolidate the following transmetalation process[40-42]. Thus, the stoichiometric reaction (Fig. 2b) of **B** with an equimolar of **2** in the presence of CuI and base produced **3b** in 89% yield, supporting **B** is the oxidative intermediate of the catalysis. As expected, the catalytic amount of **B** can promote the reaction effectively in a high yield of 89% (Fig. 2c). Moreover, the conversion of **3b** dropped significantly to 12-9% yields in the absence of CuI, signifying the importance of CuI salt.

To probe the role of copper salts, a series of deuteration experiments were performed (Fig. 2d). Apparently, base is the obligatory composition to realize the deuteration, since no benzo[*b*]thiophene-2-*d* (**2-*d***) was obtained in the absence of the base (Supplementary Table 3). Without $Pd_2(dba)_3$, the **2-*d*** dropped slightly from 80% to 73% (entries 1-2, Fig. 2d), suggesting the Pd catalyst plays no key role in this reaction. However, the yields significantly dropped to *ca* 50% without either CuI or ligand (entries 3-4, Fig. 2d), highlighting the importance of CuI and the ligand. In the absence of $Pd_2(dba)_3$, CuI, and the ligand, the yield of **2-*d*** further decreased to 47% (entry 5, Fig. 2d).

According to the above results, a catalytic cycle was tentatively proposed (Fig. 3). The reaction commences from the oxidation of aryl thioether **1b** with the palladium (0) precursor Pd^0(dcype), affording the palladium (II) complex **B**. Meanwhile, the deprotonation of aryl **2** with copper (I) catalyst **F**, originated from base, dcype, and CuI, possibly produces Cu (I) complex **C**[35,36]. Then the transmetalation between **B** and **C** generates the metal intermediate complexes **D** and **E**. Finally, the **D** undergoes reductive elimination to regenerate Pd^0(dcype) and produce the target biaryl **3b**. Meanwhile, copper (I) complex **E** proceeds via ligands exchange to regenerate **F**.

Kinetic Studies

With **2-*d*** in hand, a kinetic isotope experiments (KIE) of two parallel reactions showed no obvious kinetic isotope effect (k_H/k_D = 1.13; *k*, rate constant) (Fig. 2e), indicating that C-H bond cleavage is not the turnover-limiting step in the catalytic cycle[43]. Next, the kinetic studies via variable time normalization analysis (VTNA)[44,45] were performed to determine the order of the reaction components. As shown in Fig.

4, the order of 0 was obtained for both reactants **1b** (Fig. 4a) and **2** (Fig. 4b), indicating neither deprotonation nor oxidative addition was the turnover-limiting step. Given that the CuI is fully soluble in the solvent, the order of 0 at loadings between 10 and 20 mol% (Fig. 4c) implies that the above Cu-catalytic cycle is not rate limiting, in accordance with the KIE results. Subsequently, the order of 0.5 kinetic profiles was observed for [Pd(P^tBu_3)$_2$/dcype] (Fig. 4d), signifying the turnover-limiting step of Pd-catalyzed cycle. Meanwhile, the order of 1.5 kinetic profiles were observed for Pd(P^tBu_3)$_2$ at loadings between 5 and 10 mol% (Fig. 4e) and for dcype at loadings between 7.5 and 10 mol% (Fig. 4f), indicating an additional resting state of Pd(P^tBu_3)$_2$ existed due to the reversible coordination reaction from the Pd^0(dcype)[46,47]. After ruling out the oxidative addition and transmetalation, we can conclude that the reduction elimination is the turnover-limiting step.

DFT Calculation Studies

To corroborate the experimentally derived catalytic mechanisms, density functional theory (DFT) calculations were performed at B3LYP-D3(BJ)/BSI level to evaluate the energetic feasibility of the reaction pathways using **1b** and **2** as model compounds (see Supplementary Section IX for computational details). The energy profile for the reaction of **2** and **1b** is shown in Fig. 5. To begin with, the reaction system first undergoes initiation, resulting in a Pd(0) active species **I** and a Cu(I) active species **F**, respectively, which starts the Pd/Cu dual catalysis. Supportively, the initiation processes are energetically favorable (Supplementary Fig. 27). Subsequently, the Pd(0) species **I** undergoes oxidative addition to break C-S bond of **1b** via **TS-1**, while the Cu(I) species **F** activates the C-H bond of **2** via metathesis described by **TS-2**. Both substrate activations are kinetically feasible with a barrier around 15.0 kcal/mol, but note that the activation of **1b** is much more exergonic than that of **2** (-14.5 versus -1.8 kcal/mol). The activation energetics well explains why the oxidative addition species **B** of **1b** was easily isolated rather than the C-H activation species **C** of **2** (Fig. 5). Subsequent to the substrate activations, the resultant two species (**C** and **B**) undergo transmetalation via **TS-3**, leading to the diarylpalladium intermediate **D**. The transmetalation could be observed by the structural evolution from **IV** to **TS-3**, which indicates that the migration of SMe group from Pd- to Cu-center, and that of the aryl group of **2** from Cu- to Pd-center. Finally, the reductive elimination proceeds via **TS-4**, delivering the coupling product **3b** and regenerating the Pd(0) active species **I**. On the other hand, the thioether copper intermediate **E** from transmetalation could favorably react with KO^tBu to regenerate copper active species **F** (Supplementary Fig. 29). Thus, both active catalysts could be regenerated for the Pd/Cu dual catalysis. Overall, the reaction is exergonic by 27.6 kcal/mol with a rate-determining barrier (20.8 kcal/mol) for reductive elimination step, energetically demonstrating the occurrence of the reaction. Notably, the higher reductive elimination barrier than the C-H activation barrier of **2** (15.5 kcal/mol) also agreed with our kinetic isotope effect experiment that measured a k_H/k_D =1.13 (Fig. 2e). In addition, our calculations suggest that the C-H bond activation at the C2-position of **2** is more easily than that at the C3-position (with a barrier of 15.5 *versus* 16.5 kcal/mol, Supplementary Fig. 30), explaining the regioselectivity of the reaction.

Optimization of Polycondensation Reaction Conditions

With the success of the small molecule reactions, a challenging C-S bond activation based DArP (CAS-DArP) was initially investigated upon choosing 4,8-bis((2-hexyldecyl)oxy)benzo[1,2-*b*:4,5-*b*']dithiophene-2,6-bis(methylthio) (**E1**) and 2,2'-bithiophene (**N1**) as coupling partners for the synthesis of polymer **P1**. Table 2 summarized the optimizing reaction conditions. Under the condition of catalytic $Pd_2(dba)_3$, CuI, base, and dcype in toluene, the polymer **P1** with M_n of 16.5 kg/mol and of 1.66 was obtained in 68% yield (entry 1; Table 2). After simple screening of the Pd catalysts (entries 2-4), $Pd(MeCN)_2Cl_2$ in a high loading of 20 mol% provided the best conversion (98%) of polymer **P1** with M_n up to 51.6 kg/mol. After reducing the loading of $Pd(MeCN)_2Cl_2$ (entries 5-6), the M_n of **P1** dramatically decreased. Next, the high boiling point solvents including *o*-xylene and chlorobenzene were scrutinized (entries 7-8), showing much lower reactivity than the reaction in toluene. Finally, several control polymerizations by lowing concentrations (entries 9-10) or shortening the reaction time (entry 11) resulted in the significant decrease of M_ns and yields. Therefore, entry 4 is the optimal condition for the cross-coupling polymerization.

Substrate Scope

To investigate the generality of this DArP method, a broad array of (hetero)aryls (**N1-N10**) and (hetero)aryl thioethers (**E1-E8, M1-M5**) scope (Supplementary Fig. 14) were scrutinized to illustrate this polycondensation protocol. Fig. 6 summarized all polymerization results under the optimal or fine-tuned reaction conditions. First, to probe the universality of the aryl thioether electrophiles, 4,8-bis(octadecyloxy)benzo[1,2-*b*:4,5-*b*']dithiophene-2,6-bis(methylthio) (**E2**), 4,8-bis(4,5-didodecylthiophen-2-yl)benzo[1,2-*b*:4,5-*b*']dithiophene-2,6-bis(methylthio) (**E3**), and 5,5'''-bis(methylthio)-3,3'''-bis(2-octyldodecyl)-2,2':5',2'':5'',2'''-quaterthiophene (**E4**) were cross-coupled with **N1** to afford **P2**, **P3**, and **P4**, respectively, with high molecular weights (M_n = 30.3-76.0 kg/mol) and yields (83-98%), suggesting excellent generality of thioethers for polymerization. Not surprisingly, the side chains play important roles on the molecular weights of the polymers due to the solubility limitation[48]. Thus, the molecular weight of **P3** (M_n = 76.0 kg/mol) with aryl alkyl chains is higher than that of **P1** (M_n = 51.6 kg/mol) with branched alkyl chains. When the side chains changed to linear alkyl chains, the molecular weight of **P2** is further reduced to 30.3 kg/mol. Impressively, the **P3** was able to be synthesized in gram scale, revealing the robustness of this methodology and potential for future large-scale commercialization. To further extend the scope from thiophene thioethers and phenyl thioethers, using $Pd(P^tBu_3)_2$ as the catalyst, an aryl 4,4,9,9-tetrahexadecyl-4,9-dihydro-*s*-indaceno[1,2-*b*:5,6-*b*']dithiophene (**N2**) was employed to cross-couple with 2,5-bis(5-(methylthio)-3-tetradecylthiophen-2-yl)thieno[3,2-*b*]thiophene (**E5**), 1,4-bis(methylthio)benzene (**E6**), 4,4'-bis(methylthio)-1,1'-biphenyl (**E7**) and 2,8-bis(methylthio)dibenzo[*b,d*]thiophene (**E8**) to afford **P5**-**P8**, respectively, in excellent yields (93-96%) with high M_ns ranging from 16.7 to 50.9 kg/mol. Similarly, the side chains effects on the polymerization significantly influence the solubility and thus molecular weight of the resulting polymers.

Next, the attention was focused on the nucleophilic (hetero)aryls. The electrophile **E1** was selected to copolymerize with 2,2'-biselenophene (**N3**), electron rich 3,3'-bis(pentyloxy)-2,2'-bithiophene (**N4**), (*E*)-1,2-di(thiophen-2-yl)ethene (**N5**), and slightly electron-poor 3,3'-difluoro-2,2'-bithiophene (**N6**) to produce **P9-P12** in excellent yields (70-98%). Especially, two high molecular weight polymers **P10** and **P11** were achieved with M_ns of 110.9 and 61.7 kg/mol, indicating the contributions from the high C-H activation reactivity of electron-rich (hetero)aryls and good solubility of the resulting polymers[49,50]. Since fused rings are commonly utilized in the semiconducting materials[51,52], the well-known building blocks benzo[1,2-*b*:4,5-*b'*]dithiophene (**N7**), 2,5-bis(3-tetradecylthiophen-2-yl)thieno[3,2-*b*]thiophene (**N8**), 2,2'-(9,9-dioctyl-9*H*-fluorene-2,7-diyl)dithiophene (**N9**) are cross-coupling with **E2**, yielding **P13-P15** with high M_ns of 15.1-25.9 kg/mol, of which **P13** was polymerized by $Pd(P^tBu_3)_2$ catalyst. Meanwhile, **E3** were selected to cross couple with electron deficient 2,2'-bithiazole (**N10**), producing **P16** with a M_n of 11.6 kg/mol, suggesting the low reactivity for activating electron deficient arenes. Additionally, one random polymer **P17** was synthesized with high M_n of 17.9 kg/mol in an excellent yield of 92%. In addition to the high reactivity of cross-coupling copolymerization, this method also presents excellent efficiency in homopolymerization. A series of aryl monothioethers were selected as the monomers for homocoupling polycondensations. Delightfully, 3,3'-dihexyl-5-(methylthio)-2,2'-bithiophene (**M1**), 5-(methylthio)-3,3'''-bis(2-octyldodecyl)-2,2':5',2'':5'',2'''-quaterthiophene (**M2**), 2-(9,9-dioctyl-7-(thiophen-2-yl)-9*H*-fluoren-2-yl)-5-(methylthio)thiophene (**M3**), and 4,8-bis((2-hexyldecyl)oxy)benzo[1,2-*b*:4,5-*b'*]dithiophene-2-(methylthio) (**M4**), as the monomers in a high concentration of 0.4 M produced high quality homopolymers **P18-P21**, respectively, in excellent yields (>95%) with narrow polydispersity indexes (~1.5) and high M_ns (33.6-85.1 kg/mol). Also, (*E*)-5'-(2-(3',4-didodecyl-[2,2'-bithiophen]-5-yl)vinyl)-3,4'-didodecyl-5-(methylthio)-2,2'-bithiophene (**M5**, 0.2 M) was polymerized with $Pd(P^tBu_3)_2$ as the catalyst to afford **P22** with 67.4 kg/mol and a slightly broad of 1.80,

which shows much higher polymerization efficiency than the same polymer synthesized in Stille polycondensation[53,54]. To understand the mechanism for the homocoupling reaction, the kinetic studies on the correlation between the M_ns and values as a function of monomer conversion in the synthesis of polymer **P18** were performed as shown in Supplementary Fig. 15. It is of note that the M_n value increased sharply at a high conversion of monomer, while the values slowly approached 2.00, suggesting a typical step-growth polycondensation[55,56]. Furthermore, the optical, electrochemical, and thermal properties of all above polymers were discussed to signify the potential applications (Supplementary Fig. 16-18, Supplementary Table 5).

Finally, a direct comparison among the classic Stille, DArP, and the present CAS-DArP were performed to synthesize the **P3** in parallel (Supplementary Table 6). Replacing the aryl sulfide substrate (**E3**) with 2,6-dibromo-4,8-bis(4,5-didodecylthiophen-2-yl)benzo[1,2-*b*:4,5-*b'*]dithiophene as the electrophile, the classic DArP afforded **P3-DArP** with a much lower M_n (15.8 kg/mol) and yield (~80%) (entry 2, Supplementary Table 6), which may be ascribed to homocoupling reaction of aryl bromide (Supplementary Fig. 19)[57-59]. Replacing the aryl with aryl distannanes, the classic Stille polymerization afforded **P3-Stille** with a

relatively lower M_n of 66.6 kg/mol and a broader Đ (2.87) than that synthesized by CAS-DArP (entry 3, Supplementary Table 6). Furthermore, **P22** was also chosen to be synthesized by coupling (*E*)-1,2-bis(3-dodecyl-5-(trimethylstannyl)thiophen-2-yl)ethene and 5,5'-dibromo-4,4'-didodecyl-2,2'-bithiophene in classic Stille reaction, which afforded **P22-Stille** with a good molecular weight (M_n of 49.0 kg/mol, Đ of 1.77) (Supplementary Table 7)[53,54]. The **P22** based OFETs demonstrated an excellent mobility of 1.35 $cm^2 V^{-1} s^{-1}$ (Supplementary Table 9), higher than the **P22-Stille** based ones (1.09 $cm^2 V^{-1} s^{-1}$). After examining the ^1H NMR of **P22-Stille** and **P22** in aromatic region, the extra peaks at 7.23-7.57 ppm for **P22-Stille** (Supplementary Fig. 21) were barely observed in that of **P22**, suggesting **P22** contains less structural defects than **P22-Stille**. Additionally, the energetic profile of trap density of states (tDOS) of **P22** and **P22-Stille** by thermal admittance spectroscopy (TAS) analysis quantify the reduction of trap states. The tDOS was on the level of 10^{16} cm^{-3} eV^{-1} for **P22** film, much smaller than that of **P22-Stille** (10^{17} cm^{-3} eV^{-1}) within the deep energy depth of around 0.35 eV in the films (Supplementary Fig. 24). Next, two-dimensional grazing-incidence wide-angle X-ray scattering (2D-GIWAXS) of **P22** reflected more ordered crystallinity than **P22-Stille** (Supplementary Fig. 26), consistent with the charge transport mobilities. These results revealed that the CAS-DArP is a good choice to the classic Stille and DArP in synthesizing CPs.

Conclusions

In summary, a robust DArP method via C-S bond cleavage (CAS-DArP) was exploited using Pd/Cu cocatalysts. The scope of aryl thioethers and aryls are versatile, exemplifying with over twenty CPs including copolymers, homopolymers and random polymers. Impressively, a mechanism was proposed based on deuterium experiments, kinetic studies, DFT calculations, and an oxidative addition intermediate confirmed with single crystal X-ray diffraction, which revealed that both Pd and Cu catalysts played critical role in the bicyclic catalysis. More importantly, CPs synthesized in this method possessed less trap densities, higher M_ns and charge transport mobility than those by the classic methods, signifying an efficient method in synthesizing CPs.

Methods

General procedure for C-H/C-S activation reaction

In a Schlenk flask under nitrogen atmosphere, a solvent (2.0 mL) of a mixture of compound **1a** (42.9 mg, 0.2 mmol) or **1b** (24.8 mg, 0.2 mmol), **2** (26.9 mg, 0.2 mmol), palladium source (if applicable), copper source (if applicable), phosphine ligand (if applicable), base (if applicable) was stirred at 120°C for 24 h. After quenching the reaction, anthracene (35.6 mg, 0.20 mmol) in toluene (20.0 mL) was added into the reaction mixture. Then the solution was filtered through celite, washed with DCM and petroleum ether (1:1 *v/v*), and analyzed via GC using anthracene as an internal standard.

General procedure for C-H/C-S copolycondensation reaction (P1-P16)

Under nitrogen atmosphere, a mixture of monomers **E1-E8** (0.20 mmol, 1 equiv), **N1-N10** (0.20 mmol, 1 equiv), $Pd(MeCN)_2Cl_2$ (10.38 mg, 0.04 mmol, 20 mol%) or $Pd(P^tBu_3)_2$ (20.44 mg, 0.04 mmol, 20 mol%), CuI (15.24 mg, 0.08 mmol, 40 mol%), dcype (16.90 mg, 0.04 mmol, 20 mol%), and KO^tBu (67.33 mg, 0.60 mmol, 3.0 equiv) were dissolved in toluene (0.5-1.0 mL) in a Schlenk tube. The reaction was stirred at room temperature for 5 min and then heated at 120°C for 48 h. After cooling to room temperature, the mixture was poured into chilled methanol (100.0 mL) for precipitation. The crude polymer was collected by filtration and purified by successive Soxhlet extraction with acetone, hexane, and chloroform. Next, the chloroform fraction was filtered through a short silica gel (chloroform), concentrated and precipitated in methanol, dried over vacuum. Finally, the desired polymer was obtained.

General procedure for the synthesis of P17

Under nitrogen atmosphere, a mixture of **E1** (53.43 mg, 0.07 mmol), **E2** (57.36 mg, 0.07 mmol), **N8** (97.61 mg, 0.14 mmol), $Pd(MeCN)_2Cl_2$ (7.26 mg, 0.028 mmol), CuI (10.67 mg, 0.056 mmol), dcype (11.83 mg, 0.028 mmol), and KO^tBu (47.13 mg, 0.42 mmol) were dissolved in toluene (0.7 mL) in a Schlenk tube. The reaction was stirred at room temperature for 5 min and heated at 120°C for 48 h. After cooling to room temperature, the mixture was poured into chilled methanol (100.0 mL) for precipitation. Then, the crude polymer was collected by filtration and purified by successive Soxhlet extraction with acetone, hexane, and chloroform. Next, the chloroform fraction was filtered through a short silica gel (chloroform), concentrated and precipitated in methanol, dried over vacuum. Finally, the desired polymer was obtained.

General procedure for C-H/C-S homopolycondensation reaction (P18-P22)

Under nitrogen atmosphere, a mixture of a **M1-M5** (0.40 mmol, 1 equiv), $Pd(MeCN)_2Cl_2$ (20.76 mg, 0.08 mmol, 20 mol%) or $Pd(P^tBu_3)_2$ (40.88 mg, 0.08 mmol, 20 mol%), CuI (30.47 mg, 0.16 mmol, 40 mol%), dcype (33.81 mg, 0.08 mmol, 20 mol%), and KO^tBu (134.66 mg, 1.20 mmol, 3.0 equiv) were dissolved in toluene (1.0 or 2.0 mL) in a Schlenk tube. The reaction was stirred at room temperature for 5 min and then heated to 120°C for 48 h. After cooling to room temperature, the mixture was poured into chilled methanol (100.0 mL) for precipitation. Then, the crude polymer was collected by filtration and purified by successive Soxhlet extraction with acetone, hexane and chloroform. Next, the chloroform fraction was filtered through a short silica gel (chloroform), concentrated and precipitated in methanol, dried over vacuum. Finally, the desired polymer was obtained.

Declarations

Data availability

All relevant data supporting the findings of this study are available in this paper and its Supplementary Information. Synthetic procedures and characterization for all the new compounds, description of the computational study and all copies of NMR spectra and GPC traces are provided in the Supplementary Information. Data for the X-ray crystal structures of **B** are available free of charge from the Cambridge Crystallographic Data Centre (https://www.ccdc.cam.ac.uk/structures/) under reference numbers CCDC 2203415, respectively. All data are available from the corresponding author upon reasonable request.

Author Contributions

H.H. and Q.S. conceived the work. M.Z. conducted the synthetic experiments and characterization. B.Z. and Z.W. performed the DFT calculation. Q.L., performed the device fabrication and analysis. Z.J., F.Z., performed the AFM test. J.Z., Z.W., performed the 2D-GIWAXS test. Y.L, Y.L., performed the tDOS test. M.Z., S.P., and X.H. conducted the FT-IR characterization. M.Z., H.X., X.Z., and X.L. synthesized monomers. M.Z., Q.S., and H.H. wrote the manuscript. H.H. provided overall supervision.

Competing interests

The authors declare no competing financial interest.

Acknowledgements

The authors acknowledge the financial support from the NSFC (52173187, 21774130, 51925306, and 52222309), National Key R&D Program of China (2018FYA 0305800), Key Research Program of the Chinese Academy of Sciences (XDPB08-2), the Strategic Priority Research Program of Chinese Academy of Sciences (XDB28000000), and Fundamental Research Funds for the Central University.

References

1. Zhao, W., He, Z. & Tang, B. Z. Room-temperature phosphorescence from organic aggregates. Nat. Rev. Mater. 5, 869–885 (2020).
2. Wang, J. *et al.* The principles, design and applications of fused-ring electron acceptors. Nat. Rev. Chem. 6, 614–634 (2022).
3. Hou, J., Inganas, O., Friend, R. H. & Gao, F. Organic solar cells based on non-fullerene acceptors. Nat. Mater. 17, 119–128 (2018).
4. Liu, C., Wang, K., Gong, X. & Heeger, A. J. Low bandgap semiconducting polymers for polymeric photovoltaics. Chem. Soc. Rev. 45, 4825–4846 (2016).
5. Liu, Y. *et al.* All-organic thermally activated delayed fluorescence materials for organic light-emitting diodes. Nat. Rev. Mater. 3, 18020 (2018).
6. Fratini, S. *et al.* Charge transport in high-mobility conjugated polymers and molecular semiconductors. Nat. Mater. 19, 491–502 (2020).

7. Chen, J., Yang, J., Guo, Y. & Liu, Y. Acceptor Modulation Strategies for Improving the Electron Transport in High-Performance Organic Field-Effect Transistors. Adv. Mater. 34, 2104325 (2022).
8. Gumyusenge, A. *et al.* Semiconducting polymer blends that exhibit stable charge transport at high temperatures. Science 362, 1131–1134 (2018).
9. Sakamoto, J., Rehahn, M., Wegner, G. & Schluter, A. D. Suzuki Polycondensation: Polyarylenes a la Carte. Macromol. Rapid Commun. 30, 653–687 (2009).
10. Lee, J. *et al.* Donor–acceptor conjugated ladder polymer via aromatization-driven thermodynamic annulation. Polym. Chem. 9, 1603–1609 (2018).
11. Carsten, B. *et al.* Stille polycondensation for synthesis of functional materials. Chem. Rev. 111, 1493–1528 (2011).
12. Yokozawa, T. & Ohta, Y. Transformation of Step-Growth Polymerization into Living Chain-Growth Polymerization. Chem. Rev. 116, 1950–1968 (2016).
13. Kukhta, N. A., Marks, A. & Luscombe, C. K. Molecular Design Strategies toward Improvement of Charge Injection and Ionic Conduction in Organic Mixed Ionic-Electronic Conductors for Organic Electrochemical Transistors. Chem. Rev. 122, 4325–4355 (2022).
14. Mayhugh, A. L., Yadav, P. & Luscombe, C. K. Circular Discovery in Small Molecule and Conjugated Polymer Synthetic Methodology. J. Am. Chem. Soc. 144, 6123–6135 (2022).
15. Okamoto, K. *et al.* C–H Arylation Reaction: Atom Efficient and Greener Syntheses of π-Conjugated Small Molecules and Macromolecules for Organic Electronic Materials. Macromolecules 46, 8059–8078 (2013).
16. Pouliot, J. R. *et al.* Direct (Hetero)arylation Polymerization: Simplicity for Conjugated Polymer Synthesis. Chem. Rev. 116, 14225–14274 (2016).
17. Wakioka, M. & Ozawa, F. Highly Efficient Catalysts for Direct Arylation Polymerization (DArP). Asian J. Org. Chem. 7, 1206–1216 (2018).
18. Kowalski, S. *et al.* Direct arylation polycondensation as simplified alternative for the synthesis of conjugated (co)polymers. Prog. Polym. Sci. 38, 1805–1814 (2013).
19. Ye, L. & Thompson, B. C. Improving the efficiency and sustainability of catalysts for direct arylation polymerization (DArP). J. Polym. Sci. 60, 393–428 (2022).
20. Li, B. J. *et al.* Cross-coupling of aryl/alkenyl pivalates with organozinc reagents through nickel-catalyzed C-O bond activation under mild reaction conditions. Angew. Chem. Int. Ed. 47, 10124–10127 (2008).
21. Wang, Y. *et al.* (Semi)ladder-Type Bithiophene Imide-Based All-Acceptor Semiconductors: Synthesis, Structure–Property Correlations, and Unipolar n-Type Transistor Performance. J. Am. Chem. Soc. 140, 6095–6108 (2018).
22. Park, J. K. *et al.* End-capping effect of a narrow bandgap conjugated polymer on bulk heterojunction solar cells. Adv. Mater. 23, 2430–2435 (2011).

23. Ni, Z. *et al.* Mesopolymer synthesis by ligand-modulated direct arylation polycondensation towards n-type and ambipolar conjugated systems. Nat. Chem. 11, 271–277 (2019).
24. Zhao, B., Prabagar, B. & Shi, Z. Modern strategies for C–H functionalization of heteroarenes with alternative coupling partners. Chem. 7, 2585–2634 (2021).
25. Lou, J. *et al.* Transition-metal mediated carbon-sulfur bond activation and transformations: an update. Chem. Soc. Rev. 49, 4307–4359 (2020).
26. Dunbar, K. L., Scharf, D. H., Litomska, A. & Hertweck, C. Enzymatic Carbon-Sulfur Bond Formation in Natural Product Biosynthesis. Chem. Rev. 117, 5521–5577 (2017).
27. Ilardi, E. A., Vitaku, E. & Njardarson, J. T. Data-mining for sulfur and fluorine: an evaluation of pharmaceuticals to reveal opportunities for drug design and discovery. J. Med. Chem. 57, 2832–2842 (2014).
28. Rivero-Crespo, M. A., Toupalas, G. & Morandi, B. Preparation of Recyclable and Versatile Porous Poly(aryl thioether)s by Reversible Pd-Catalyzed C–S/C–S Metathesis. J. Am. Chem. Soc. 143, 21331–21339 (2021).
29. Krömer, M. *et al.* Chemoselective Synthesis of 4,5-Diarylpyrrolo[2,3-d]pyrimidines (6,7-Diaryl-7-deazapurines) by Consecutive Suzuki and Liebeskind-Srogl Cross-Couplings. *Eur. J. Org. Chem.* 2014, 7203–7210 (2014).
30. Prieur, V., Pujol, M. D. & Guillaumet, G. A Strategy for the Triarylation of Pyrrolopyrimidines by Using Microwave-Promoted Cross-Coupling Reactions. *Eur. J. Org. Chem.* 2015, 6547–6556 (2015).
31. Murray, S. G. & Hartley, F. R. Coordination chemistry of thioethers, selenoethers, and telluroethers in transition-metal complexes. Chem. Rev. 81, 365–414 (1981).
32. Jiang, X. F. *et al.* Hydrolytic cleavage of both CS(2) carbon-sulfur bonds by multinuclear Pd(II) complexes at room temperature. Nat. Chem. 9, 188–193 (2017).
33. Li, Z. *et al.* Efficient room temperature catalytic synthesis of alternating conjugated copolymers via C-S bond activation. Nat. Commun. 13, 144 (2022).
34. Wang, Y., Hasegawa, T., Matsumoto, H. & Michinobu, T. Significant Difference in Semiconducting Properties of Isomeric All-Acceptor Polymers Synthesized via Direct Arylation Polycondensation. Angew. Chem. Int. Ed. 58, 11893–11902 (2019).
35. Wang, Y., Wu, S. B., Shi, W. J. & Shi, Z. J. C-O/C-H Coupling of Polyfluoroarenes with Aryl Carbamates by Cooperative Ni/Cu Catalysis. Org. Lett. 18, 2548–2551 (2016).
36. Liu, C. *et al.* Bimetallic Cooperative Catalysis for Decarbonylative Heteroarylation of Carboxylic Acids via C-O/C-H Coupling. Angew. Chem. Int. Ed. 60, 10690–10699 (2021).
37. Lee, J. A. & Luscombe, C. K. Dual-Catalytic Ag–Pd System for Direct Arylation Polymerization to Synthesize Poly(3-hexylthiophene). ACS Macro Lett. 7, 767–771 (2018).
38. Lee, S. Y. & Hartwig, J. F. Palladium-Catalyzed, Site-Selective Direct Allylation of Aryl C-H Bonds by Silver-Mediated C-H Activation: A Synthetic and Mechanistic Investigation. J. Am. Chem. Soc. 138, 15278–15284 (2016).

39. Torres Gerardo, M., Liu, Y. & Arndtsen Bruce, A. A dual light-driven palladium catalyst: Breaking the barriers in carbonylation reactions. Science 368, 318–323 (2020).
40. Bismuto, A., Delcaillau, T., Müller, P. & Morandi, B. Nickel-Catalyzed Amination of Aryl Thioethers: A Combined Synthetic and Mechanistic Study. ACS Catal. 10, 4630–4639 (2020).
41. Delcaillau, T., Bismuto, A., Lian, Z. & Morandi, B. Nickel-Catalyzed Inter- and Intramolecular Aryl Thioether Metathesis by Reversible Arylation. Angew. Chem. Int. Ed. 59, 2110–2114 (2020).
42. Boehm, P. *et al.* Mechanistic Investigation of the Nickel-Catalyzed Metathesis between Aryl Thioethers and Aryl Nitriles. J. Am. Chem. Soc. 144, 13096–13108 (2022).
43. Simmons, E. M. & Hartwig, J. F. On the interpretation of deuterium kinetic isotope effects in C-H bond functionalizations by transition-metal complexes. Angew. Chem. Int. Ed. 51, 3066–3072 (2012).
44. Blackmond, D. G. Kinetic Profiling of Catalytic Organic Reactions as a Mechanistic Tool. J. Am. Chem. Soc. 137, 10852–10866 (2015).
45. Martinez-Carrion, A. *et al.* Kinetic Treatments for Catalyst Activation and Deactivation Processes based on Variable Time Normalization Analysis. Angew. Chem. Int. Ed. 58, 10189–10193 (2019).
46. Zhao, D. *et al.* Tritiation of aryl thianthrenium salts with a molecular palladium catalyst. Nature 600, 444–449 (2021).
47. Alvaro, E. & Hartwig, J. F. Resting State and Elementary Steps of the Coupling of Aryl Halides with Thiols Catalyzed by Alkylbisphosphine Complexes of Palladium. J. Am. Chem. Soc. 131, 7858–7868 (2009).
48. Lei, T., Dou, J. H. & Pei, J. Influence of alkyl chain branching positions on the hole mobilities of polymer thin-film transistors. Adv. Mater. 24, 6457–6461 (2012).
49. Doba, T. *et al.* Iron-catalysed regioselective thienyl C–H/C–H coupling. Nat. Catal. 4, 631–638 (2021).
50. Doba, T., Shang, R. & Nakamura, E. Iron-Catalyzed C-H Activation for Heterocoupling and Copolymerization of Thiophenes with Enamines. J. Am. Chem. Soc. 144, 21692–21701 (2022).
51. Zhu, C., Kalin, A. J. & Fang, L. Covalent and Noncovalent Approaches to Rigid Coplanar pi-Conjugated Molecules and Macromolecules. Acc. Chem. Res. 52, 1089–1100 (2019).
52. Yan, C. *et al.* Non-fullerene acceptors for organic solar cells. Nat. Rev. Mater. 3, 18003 (2018).
53. Kim, J. *et al.* Highly Soluble Poly(thienylenevinylene) Derivatives with Charge-Carrier Mobility Exceeding 1 $cm^2V^{-1}s^{-1}$. Chem. Mater. 23, 4663–4665 (2011).
54. Mori, T., Komiyama, H., Ichikawa, T. & Yasuda, T. A liquid-crystalline semiconducting polymer based on thienylene–vinylene–thienylene: Enhanced hole mobilities by mesomorphic molecular ordering and thermoplastic shape-deformable characteristics. Polym. J. 52, 313–321 (2019).
55. Carothers, W. H. Polymerization. Chem. Rev. 8, 353–426 (1931).
56. Flory, P. J. Fundamental Principles of Condensation Polymerization. Chem. Rev. 39, 137–197 (1946).
57. Wakioka, M., Takahashi, R., Ichihara, N. & Ozawa, F. Mixed-Ligand Approach to Palladium-Catalyzed Direct Arylation Polymerization: Highly Selective Synthesis of π-Conjugated Polymers with

Diketopyrrolopyrrole Units. Macromolecules 50, 927–934 (2017).

58. Pankow, R. M., Ye, L. & Thompson, B. C. Influence of the Ester Directing Group on the Inhibition of Defect Formation in Polythiophenes with Direct Arylation Polymerization (DArP). Macromolecules 53, 3315–3324 (2020).
59. Hendriks, K. H. *et al.* Homocoupling defects in diketopyrrolopyrrole-based copolymers and their effect on photovoltaic performance. J. Am. Chem. Soc. 136, 11128–11133 (2014).

Tables

Tables 1 to 2 are available in the Supplementary Files section

Figures

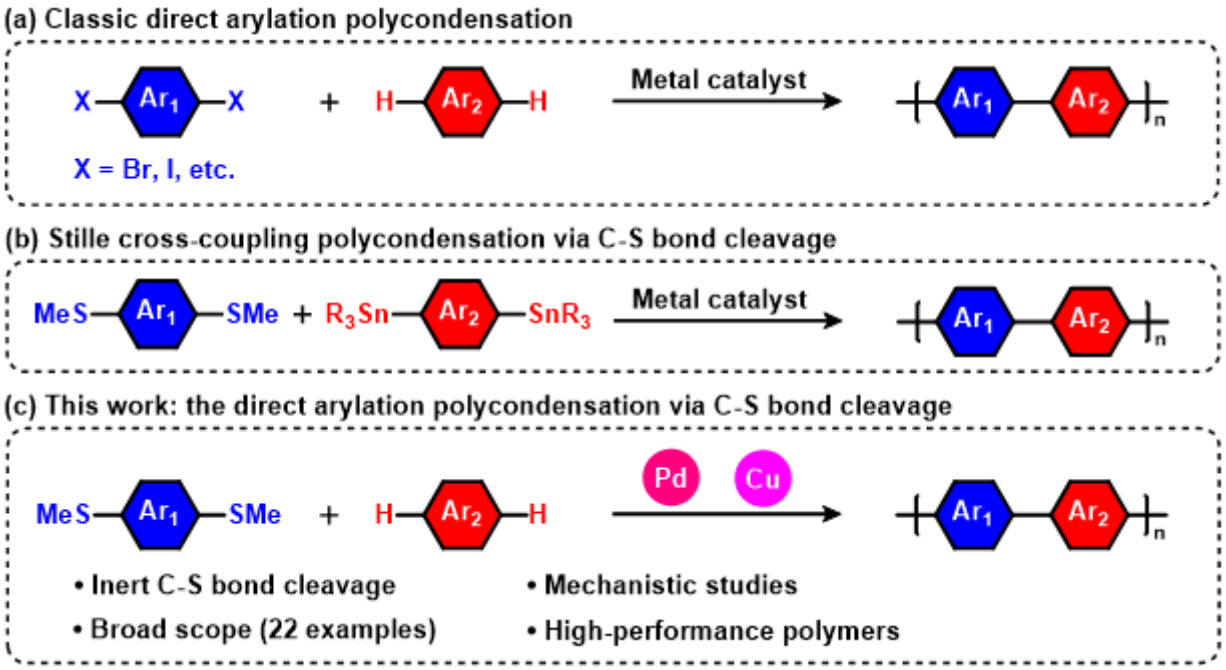

Figure 1

Motivation and development of cross-coupling reactions via C-S bond cleavage.**(a)** Classic direct arylation polycondensation. **(b)** Stille cross-coupling polycondensation via C-S bond cleavage. **(c)** The direct arylation polycondensation via C-S bond cleavage (this work).

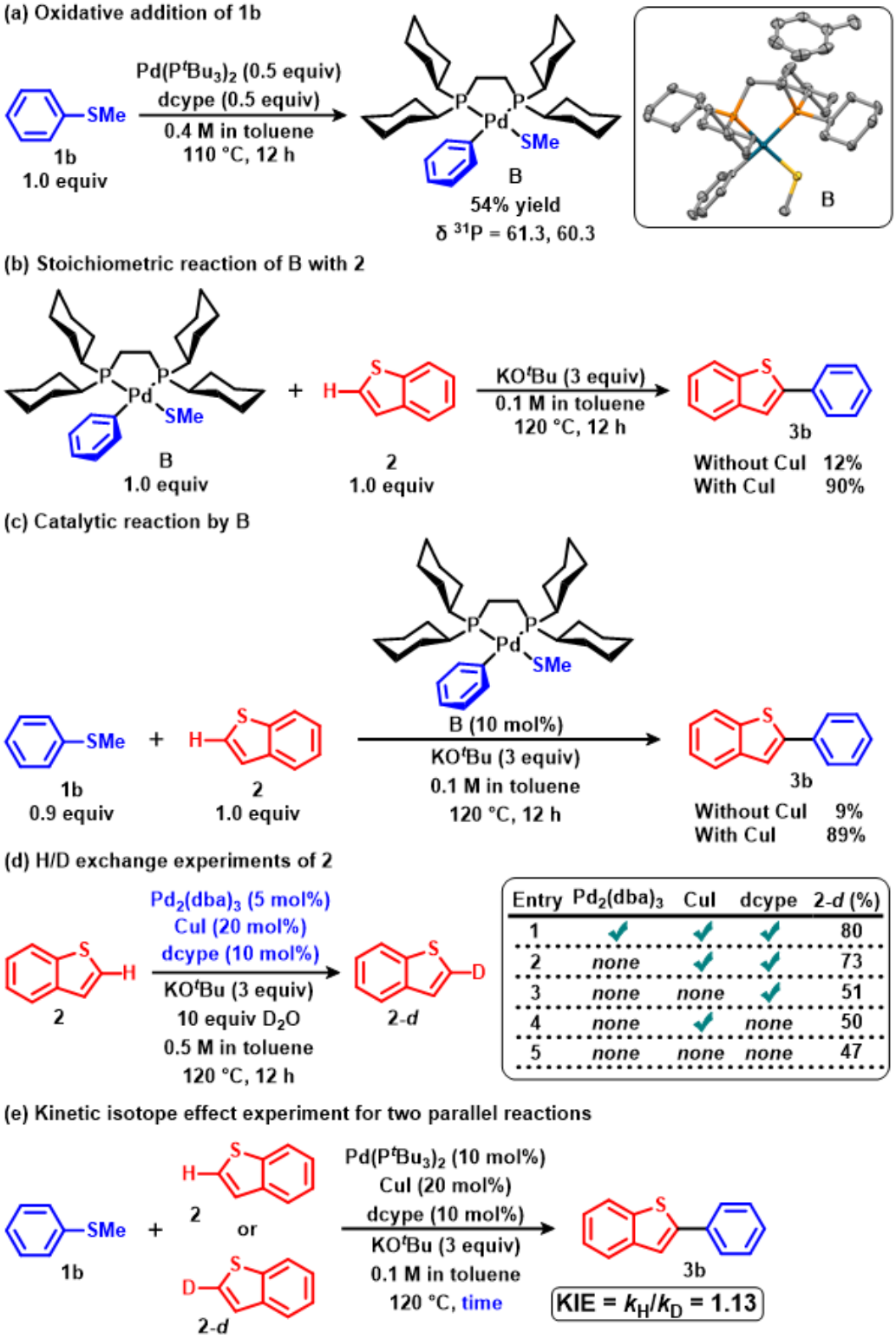

Figure 2

Mechanistic studies. **(a)** Oxidative addition of **1b** at 110 °C generates an intermediate **B**. The isolated yields. **(b)** Stoichiometric reaction of **B** with **2** at 120 °C generates a product **3b**. Yields were determined by GC using anthracene as an internal standard. **(c)** Catalytic reaction by **B** at 120 °C generates a product **3b**. Yields were determined by GC using anthracene as an internal standard. **(d)** H/D exchange experiments of **2**. For detailed data, see Supplementary Table 3. Yields were determined by ^{1}H NMR using

1,4-dimethoxybenzene as an internal standard. **(e)** Kinetic isotope effect (KIE) experiment for two parallel reactions. k_H, rate constant of **2**; k_D, rate constant of **2-*d***. Yields were determined by GC using anthracene as an internal standard.

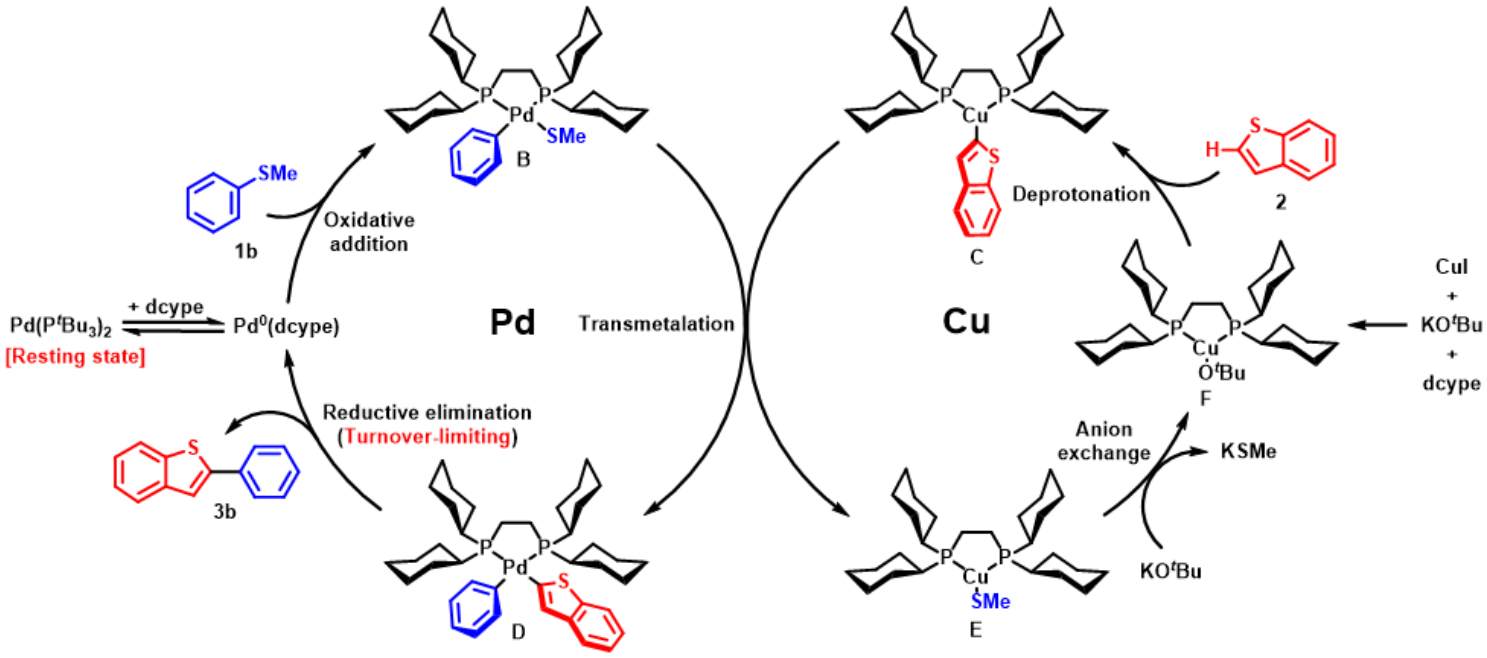

Figure 3

Proposed mechanism for C-H/C-S activation reaction.

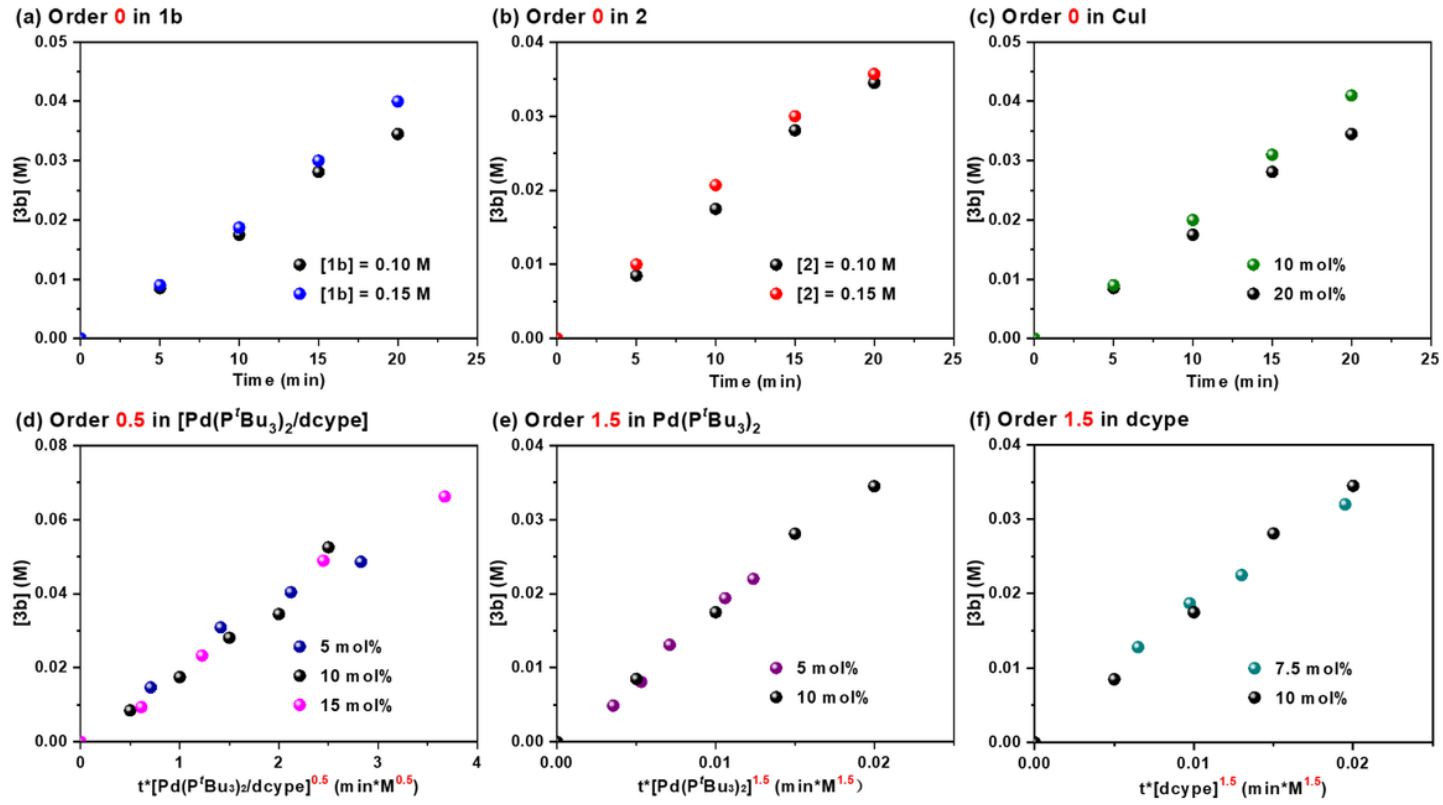

Figure 4

Kinetic studies. K inetic profiles in different concentrations of **1b (a)** and **2 (b)**. Kinetic profiles in different loadings of CuI **(c)**, [Pd(P^tBu_3)$_2$/dcype] **(d)**, Pd(P^tBu_3)$_2$ **(e)**, and dcype **(f)**. For detailed data, see Supplementary Section IV-7.

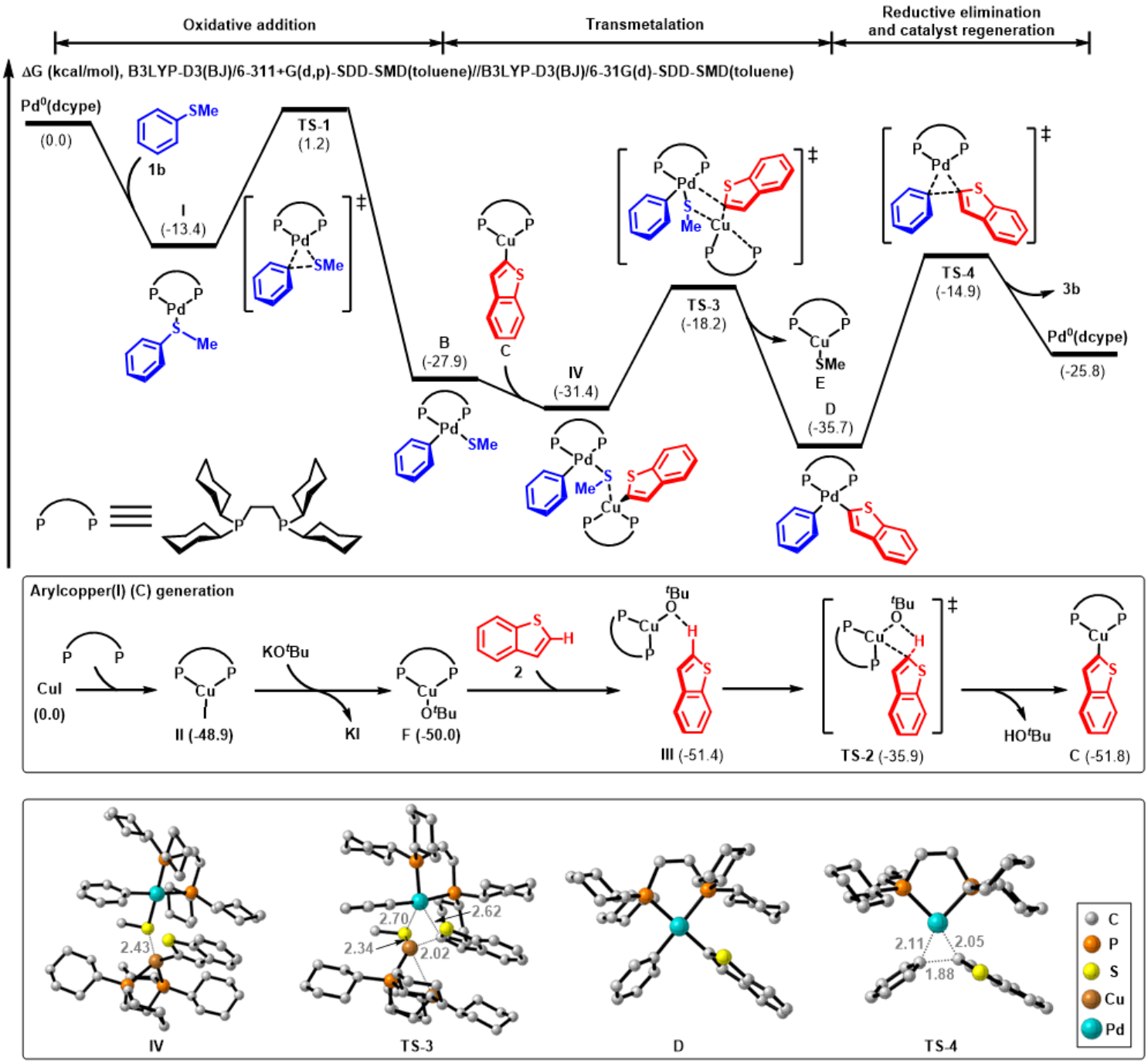

Figure 5

DFT calculation studies. Energy profile of Pd/Cu dual-catalyzed C-H/C-S activation reaction and the optimized structures of the key stationary points. Bond lengths are given in angstroms. The calculated

Gibbs energies (ΔG and $\Delta G‡$, 298.15 K, 1 atm) are shown in kcal mol^{-1}. For detailed profiles, see Supplementary Section IX.

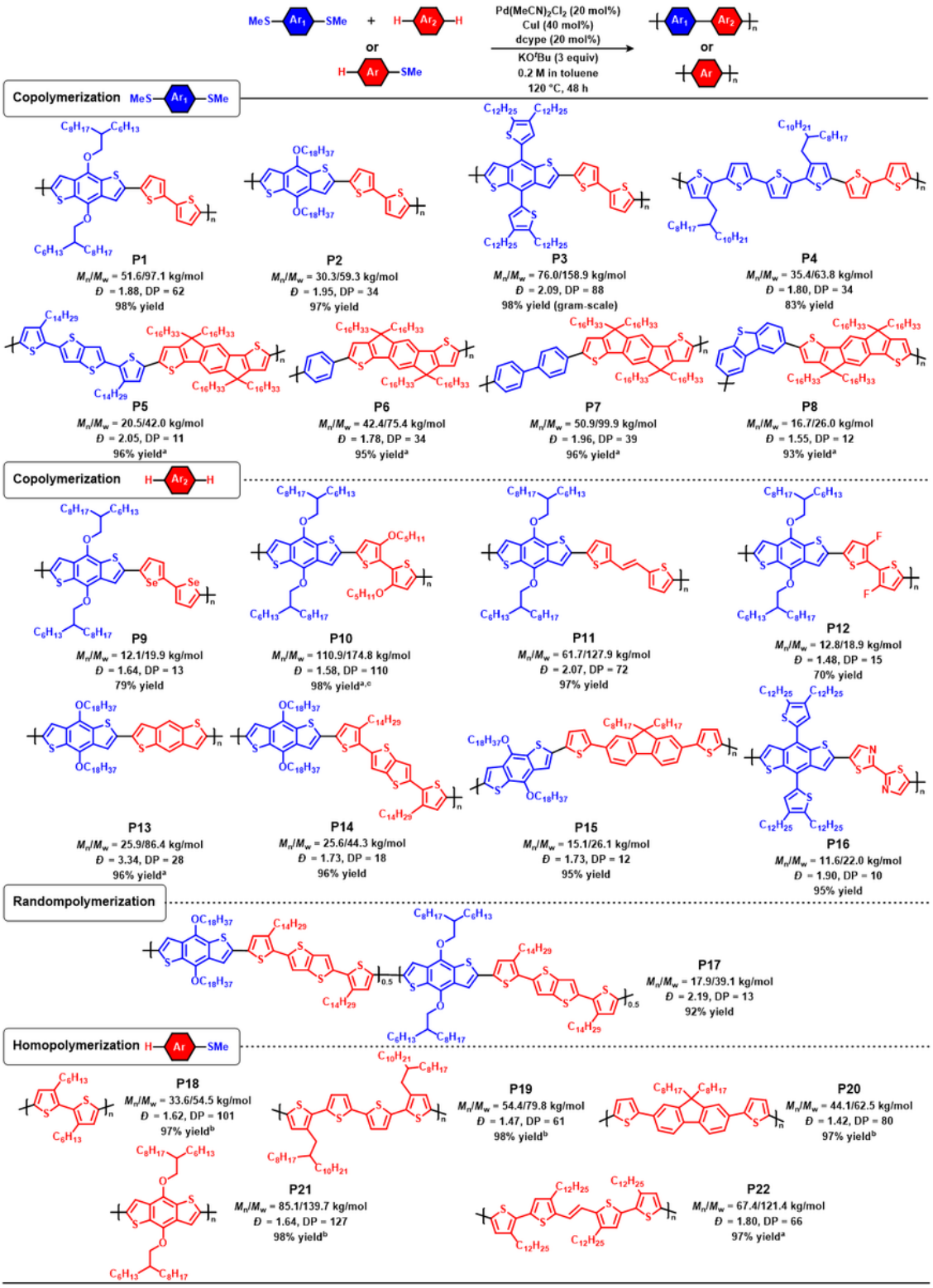

Figure 6

Substrate scope of direct arylation polycondensation via C-S bond cleavage. M_n, M_w, and were determined with GPC at 150 °C in 1,2,4-trichlorobenzene against a polystyrene standard. The degree of

polymerization was calculated using M_n. [a]The $Pd(P^tBu_3)_2$ (20 mol%) was used instead of $Pd(MeCN)_2Cl_2$ (20 mol%). [b]Reaction concentration of 0.4 M. [c]Reaction concentration of 0.3 M. For experimental details of polymers, see Supplementary Section V.

Supplementary Files

This is a list of supplementary files associated with this preprint. Click to download.

- TOC.png
- Tables.docx
- CHCSSI.pdf